J Mater Sci (2008) 43:3118–3123
DOI 10.1007/s10853-008-2504-6

# Synthesis and characterization of bulk amorphous/amorphous composite alloys through powder metallurgy route

**Hong-Ming Lin · Yu-Wei Lin · Pee-Yew Lee**

Received: 29 September 2007 / Accepted: 25 January 2008 / Published online: 28 February 2008


**Abstract** In the present study, amorphous $Ni_{60}Nb_{20}Zr_{20}$ and $Ti_{50}Cu_{28}Ni_{15}Sn_7$ alloy powders were synthesized separately using a mechanical alloying (MA) technique. The dual-amorphous-phased $(Ti_{50}Cu_{28}Ni_{15}Sn_7)_{100-x}(Ni_{60}Nb_{20}Zr_{20})_x$ ($x = 0$, 10, 20, and 30 vol%) powders were prepared by mixing the corresponding amorphous powders. The dual-amorphous-phased powders were then consolidated into bulk amorphous/amorphous composite (BA/AC) alloy discs. The amorphization status of as-prepared powders and bulk BA/AC composite discs was confirmed by X-ray diffraction (XRD) and transmission electron microscopy (TEM). The microstructure of the BA/AC discs showed that the $Ni_{60}Nb_{20}Zr_{20}$ phase is distributed homogeneously within the $Ti_{50}Cu_{28}Ni_{15}Sn_7$ matrix. The $(Ti_{50}Cu_{28}Ni_{15}Sn_7)_{70}(Ni_{60}Nb_{20}Zr_{20})_{30}$ BA/AC disc exhibited a relative density of 96.6% and its Vickers microhardness was 726 kg/mm$^2$.

## Introduction

Recently, new metallic glass with a wide supercooled liquid region has been prepared in several different alloy systems. The existence of the wide supercooled liquid region enables the formation of bulk metallic glass (BMG) by conventional casting techniques at a low cooling rates ranging from 1.5 K/s to 100 K/s. This new BMG exhibits a high hardness and yield strength, a low Young's modulus, a large elastic strain limit, and a relatively high fracture toughness as well as good wear and corrosion resistance. However, BMGs usually show little overall room temperature plasticity due to the formation of highly localized shear banding, resulting in a catastrophic failure [1]. Attempts have been made to enhance the ductility of BMGs by introducing a crystalline phase into the metallic glass matrix by partial devitrification, adding particle during casting or consolidation process, and in situ formed ductile-phase precipitates [2–4]. It was found that the existence of ceramic or insoluble metallic particles inside the glass matrix can suppress the propagation of shear bands, and therefore increase the toughness and ductility of metallic glass matrix composite. In an effort to further improve the properties of the metallic glass matrix composite, a new kind of dual-amorphous-phased BMG with amorphous/amorphous composite structure has attracted increased R&D interest. Similar to a composite material, the dual-amorphous-phased BMG can be expected to exhibit properties of both its original constituents. For instance, the relatively brittle Fe-based BMG can be improved by alloying it with high-toughness Zr-based BMG [5]. Conventional casting or mould-injection techniques can be used to prepare bulk dual-amorphous-phased alloys. For instance, it has been observed that Ni–Nb–Y [6] and Nd–Zr–Al–Co [7] alloys can undergo metastable liquid-phase separation and thus form a bulk dual-amorphous-phased alloy. However, the multicomponent alloy systems with confined constitutional range that can induce phase separation are very rare, and thus restrict

H.-M. Lin
Department of Materials Engineering, Tatung University, Taipei, Taiwan

Y.-W. Lin
Department of Materials Science and Engineering, National Cheng Kung University, Tainan, Taiwan

P.-Y. Lee (✉)
Institute of Materials Engineering, National Taiwan Ocean University, Keelung, Taiwan
e-mail: pylee@mail.ntou.edu.tw

the formation of bulk dual-amorphous-phased BMG using conventional casting or mould-injection techniques. Therefore, an alternative technique to prepare bulk dual-amorphous-phased alloys would be via powder metallurgical methods, where the amorphous alloy can be prepared individually and then consolidated into a disc by hot pressing or other appropriate processes. In the present study, the feasibility of preparing dual-phased $(Ti_{50}Cu_{28}Ni_{15}Sn_7)_{100-x}$ $(Ni_{60}Nb_{20}Zr_{20})_x$ bulk amorphous/amorphous composite (BA/AC) alloys by a combination of mechanical alloying (MA) and vacuum hot-pressing techniques was investigated. The $Ti_{50}Cu_{28}Ni_{15}Sn_7$ alloy was chosen as a matrix component because it has been well studied by our group [8]. The $Ni_{60}Nb_{20}Zr_{20}$ was selected due to its excellent thermal stability against crystallization (the crystallization temperature of the amorphous phase is 896 K).

## Experimental procedure

Amorphous $Ni_{60}Nb_{20}Zr_{20}$ and $Ti_{50}Cu_{28}Ni_{15}Sn_7$ (at%) powders were prepared by MA, starting from the elemental powder mixtures of Ni (99.9%, <300 mesh), Nb (99.8%, <325 mesh), Zr (99.5%, <100 mesh), Ti (99.7%, <325 mesh), Cu (99.9%, <325 mesh), and Sn (99.999%, 100 mesh). A SPEX 8016 double shaker ball mill was used for MA under an Ar-filled environment. The duration of the overall milling process for preparing amorphous $Ni_{60}Nb_{20}Zr_{20}$ and $Ti_{50}Cu_{28}Ni_{15}Sn_7$ powders was 8 h. The as-milled powders were confirmed to be amorphous by an analytical X'Pert PRO diffractometer using a monochromatic Cu-$K_\alpha$ radiation.

The amorphous $Ni_{60}Nb_{20}Zr_{20}$ and $Ti_{50}Cu_{28}Ni_{15}Sn_7$ powders were weighted to the desired compositions of $(Ti_{50}Cu_{28}Ni_{15}Sn_7)_{100-x}(Ni_{60}Nb_{20}Zr_{20})_x$ ($x = 0$, 10, 20, and 30 vol%), and mixed further for 2 h in the SPEX ball mill. The $(Ti_{50}Cu_{28}Ni_{15}Sn_7)_{100-x}(Ni_{60}Nb_{20}Zr_{20})_x$ composite powders were then consolidated in a vacuum hot-pressing machine at 723 K under a pressure of ~1.2 GPa for 30 min to prepare BA/AC alloy discs with a diameter of 10 mm and thickness of 4 mm. The as-milled and consolidated samples were re-examined by X-ray diffraction (XRD), differential scanning calorimeter (DSC), scanning electron microscopy (SEM), and transmission electron microscopy (TEM). The specimen for TEM examination was ground to a thickness of 150 μm. The specimen was then subjected to single-jet polishing with a 550D Single Vertical Jet Electropolisher (South Bay Technology Inc.). The polishing conditions are 15 V, −30 to −40 °C. The densities of the BA/AC alloys were measured by the Archimedean method according to ASTM standard C639 [9]. The Vickers microhardness of the consolidated BA/AC alloys samples was measured using a Matsuzawa MXT50-UL machine with a static load of 0.5 N.

## Results and discussion

### Amorphous powders

Figure 1 shows the XRD patterns of $Ni_{60}Nb_{20}Zr_{20}$ and $Ti_{50}Cu_{28}Ni_{15}Sn_7$ powders. A broad diffraction peak, attributable to the amorphous nature of the powders, can be observed at ~41° and ~42.5° for $Ni_{60}Nb_{20}Zr_{20}$ and $Ti_{50}Cu_{28}Ni_{15}Sn_7$ powders, respectively, suggested by the XRD results (Fig. 1). Figure 2 shows the corresponding TEM image with a selected area diffraction (SAD) pattern for the $Ni_{60}Nb_{20}Zr_{20}$ and $Ti_{50}Cu_{28}Ni_{15}Sn_7$ powders. For both powders, the electron diffraction pattern consists of halo rings, and the bright-field electron micrograph reveals featureless contrast, indicating the structure of the powders is a single amorphous phase. Though the TEM observation confirms the matrix of as-milled powders is a glassy phase, it is noted the XRD patterns for these samples reveal a tiny crystalline peak that was formed around $2\theta = 38°$. This implies that a small volume of the nanocrystalline phase present in the as-milled powders is possible. Figure 3 shows the powder morphology and cross-sectional view of the as-milled amorphous powders after examination by SEM. The cross-sectional view revealed that both the as-milled powders exhibited a homogeneous phase (i.e., amorphous phase). The as-milled powders were examined by XRD and SEM as a function of the milling time even though this has not been shown in this paper. The process of milling either $Ni_{60}Nb_{20}Zr_{20}$ or $Ti_{50}Cu_{28}Ni_{15}Sn_7$ powders exhibited a trend similar to that of typical amorphous alloys prepared from the elementary powder mixtures by MA [10].

The thermal stability of the amorphous $Ni_{60}Nb_{20}Zr_{20}$ and $Ti_{50}Cu_{28}Ni_{15}Sn_7$ powders was investigated using a DSC. Figure 4 shows the DSC scans of the as-milled amorphous

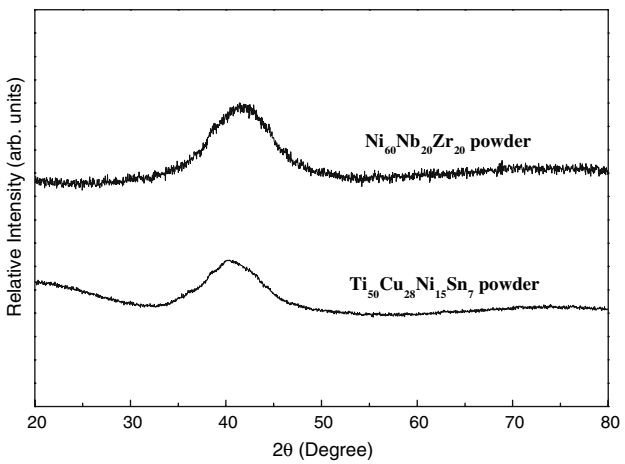


**Fig. 1** XRD patterns of amorphous $Ti_{50}Cu_{28}Ni_{15}Sn_7$ and $Ni_{60}Nb_{20}Zr_{20}$ powders

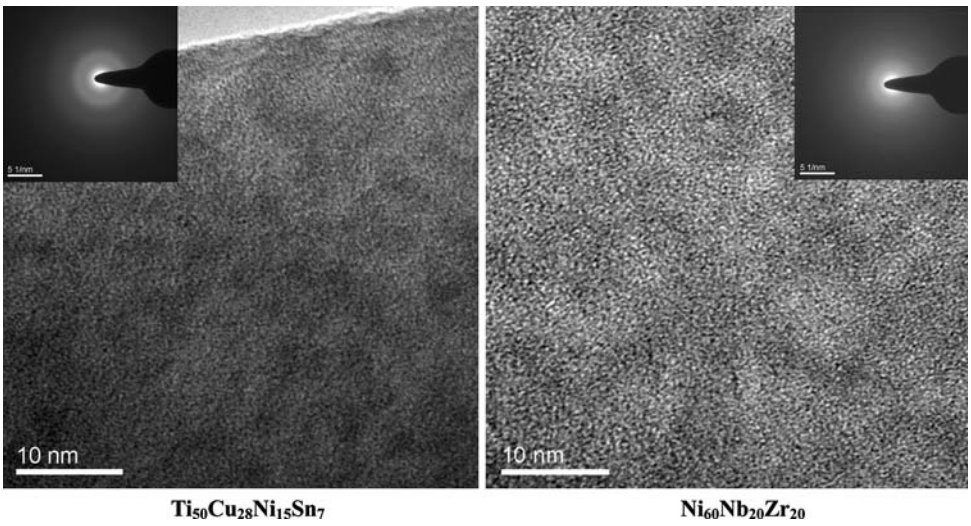


**Fig. 2** Bright-field TEM images and corresponding selected-area diffraction patterns of amorphous $Ti_{50}Cu_{28}Ni_{15}Sn_7$ and $Ni_{60}Nb_{20}Zr_{20}$ powders

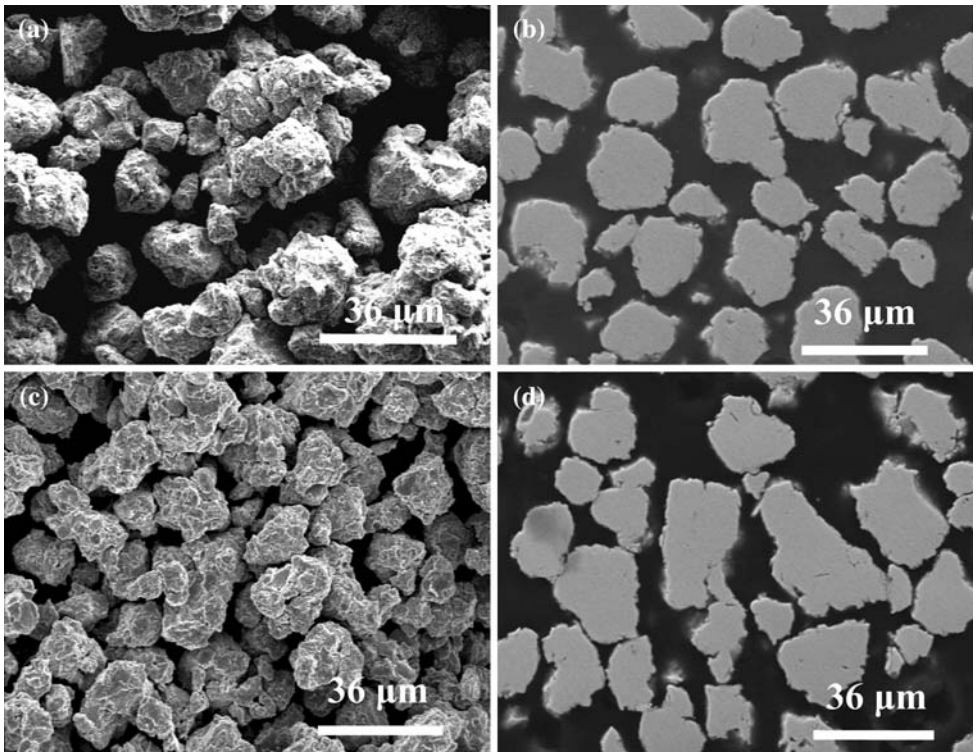


**Fig. 3** Surface morphology and cross-sectional view of amorphous $Ti_{50}Cu_{28}Ni_{15}Sn_7$ and $Ni_{60}Nb_{20}Zr_{20}$ powders. (**a**) and (**b**) are amorphous $Ti_{50}Cu_{28}Ni_{15}Sn_7$ powders, while (**c**) and (**d**) are $Ni_{60}Nb_{20}Zr_{20}$ powders

powders. It can be observed that both the $Ni_{60}Nb_{20}Zr_{20}$ and $Ti_{50}Cu_{28}Ni_{15}Sn_7$ powders exhibited an endothermic glass transition followed by a sharp exothermic peak, indicating the successive stepwise transformation from a supercooled liquid state to a crystalline phase. As shown in Fig. 4, the glass transition ($T_g$) and crystallization ($T_x$) temperatures were 855 and 896 K for the amorphous $Ni_{60}Nb_{20}Zr_{20}$ powders, and 713 and 765 K for the $Ti_{50}Cu_{28}Ni_{15}Sn_7$ powders, respectively. The relatively wide supercooled region ($\Delta T_x$, defined as $T_x - T_g$) was 41 and 52 K for the amorphous $Ni_{60}Nb_{20}Zr_{20}$ and $Ti_{50}Cu_{28}Ni_{15}Sn_7$ powders, respectively.

## Amorphous/amorphous composite powders

The amorphous $Ni_{60}Nb_{20}Zr_{20}$ and $Ti_{50}Cu_{28}Ni_{15}Sn_7$ powders (as discussed above) were weighted to the desired compositions of $(Ti_{50}Cu_{28}Ni_{15}Sn_7)_{100-x}(Ni_{60}Nb_{20}Zr_{20})_x$

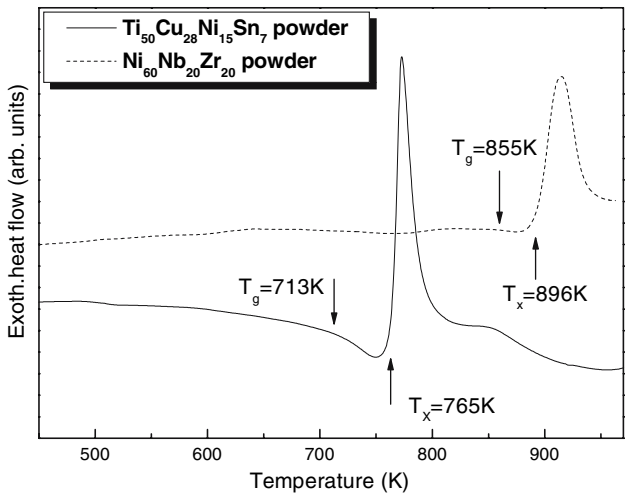


**Fig. 4** DSC curves of amorphous $Ti_{50}Cu_{28}Ni_{15}Sn_7$ and $Ni_{60}Nb_{20}Zr_{20}$ powders

($x = 0$, 10, 20, and 30 vol%), and mixed further for 2 h. The amorphization status of the composite powders was first examined by XRD. Figure 5 shows the XRD patterns of the composite powders as a function of $Ni_{60}Nb_{20}Zr_{20}$ addition. A broad diffraction peak, attributable to the amorphous nature, can be observed. Interestingly, only a single amorphous peak can be observed, and its position increased with the $Ni_{60}Nb_{20}Zr_{20}$ concentration. This characteristic differs from that reported by Park et al. [7] who prepared Nd–Zr–Co–Al BMG with dual amorphous phases for which both the amorphous peaks can be observed. The current XRD results in Fig. 5, however, exhibit a trend similar to that of the two-phase amorphous ternary Ni–Nb–Y ribbons prepared by a single-roller melt spinner [6] since the position of the broad diffraction peak is $\sim 41°$ for amorphous $Ni_{60}Nb_{20}Zr_{20}$ and $\sim 42.5°$ for amorphous $Ti_{50}Cu_{28}Ni_{15}Sn_7$, respectively. It is suggested that the

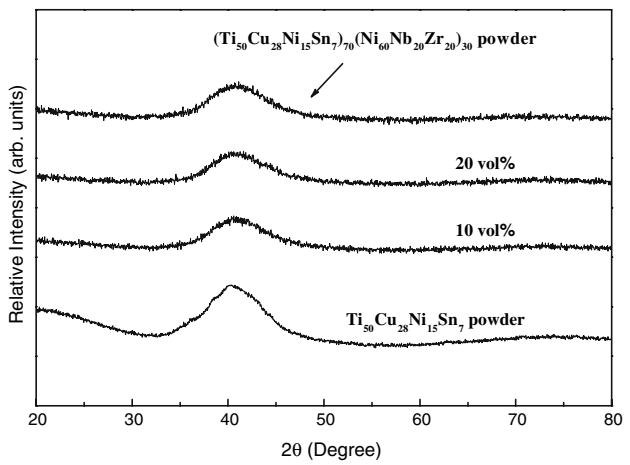


**Fig. 5** XRD patterns of composite $(Ti_{50}Cu_{28}Ni_{15}Sn_7)_{100-x}(Ni_{60}Nb_{20}Zr_{20})_x$ powders

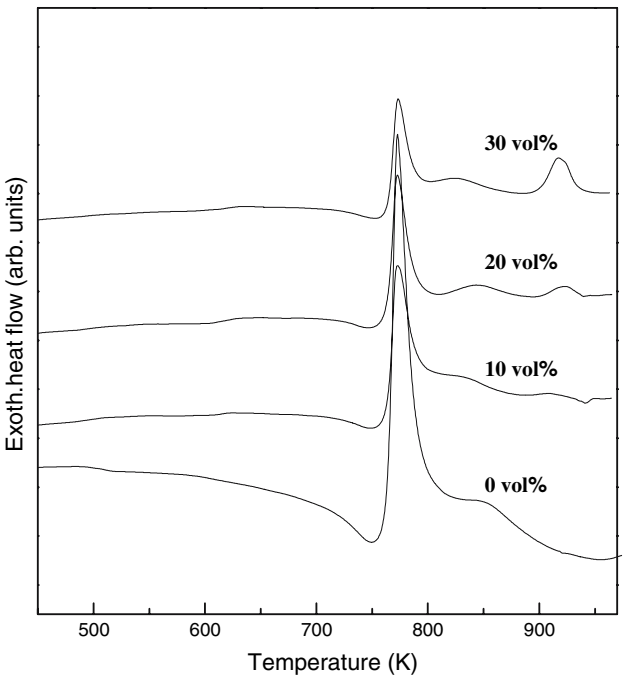


**Fig. 6** DSC curves of composite $(Ti_{50}Cu_{28}Ni_{15}Sn_7)_{100-x}(Ni_{60}Nb_{20}Zr_{20})_x$ powders

appearance of a single amorphous peak of XRD patterns of the composite powders is due to the overlapping of these broad diffraction peaks.

The thermal stability of the amorphous composite $(Ti_{50}Cu_{28}Ni_{15}Sn_7)_{100-x}(Ni_{60}Nb_{20}Zr_{20})_x$ powders was examined and Fig. 6 shows the corresponding DSC curves as a function of $Ni_{60}Nb_{20}Zr_{20}$ addition. It can be observed that the amorphous composite powders exhibited a supercooled behaviour similar to that of the amorphous $Ti_{50}Cu_{28}Ni_{15}Sn_7$ powders. In addition to the supercooled behaviour of the amorphous $Ti_{50}Cu_{28}Ni_{15}Sn_7$ phase, the corresponding responses of the amorphous $Ni_{60}Nb_{20}Zr_{20}$ powders can also be observed at 896 K. It is noted that the $T_g$ of the amorphous composite powders increases slightly with $Ni_{60}Nb_{20}Zr_{20}$ addition. The $T_x$ of the amorphous composite powders ranged from 764 K to 766 K and did not exhibit any significant differences. A decrease in the supercooled region (the difference between $T_x$ and $T_g$) due to the addition of $Ni_{60}Nb_{20}Zr_{20}$ can be observed. The DSC examinations revealed that the amorphous composite powders exhibited both the supercooled behaviour of the original amorphous $Ti_{50}Cu_{28}Ni_{15}Sn_7$ and the characteristics of $Ni_{60}Nb_{20}Zr_{20}$ and thus possessed dual amorphous phases.

## Bulk amorphous/amorphous composite (BA/AC) alloys

To successfully prepare bulk glassy samples by consolidation of the milled powders, it is important to correctly estimate the consolidation parameters (such as temperature

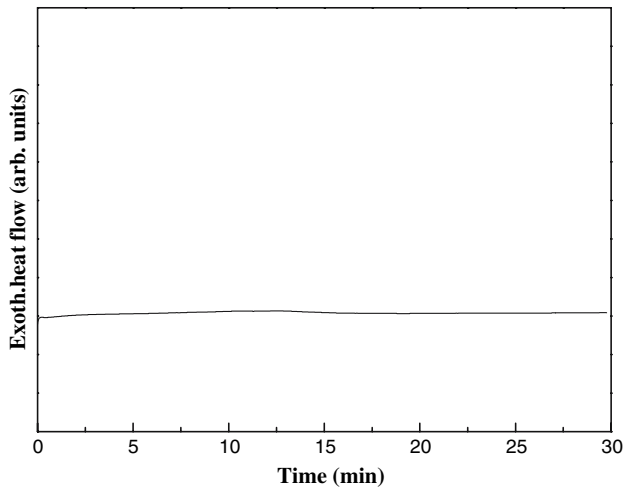


**Fig. 7** Isothermal DSC curve of dual-amorphous-phased $(Ti_{50}Cu_{28}Ni_{15}Sn_7)_{70}(Ni_{60}Nb_{20}Zr_{20})_{30}$ powders

and time) for avoiding the crystallization reaction. Thus, isothermal DSC analysis of dual-amorphous-phased $(Ti_{50}Cu_{28}Ni_{15}Sn_7)_{70}(Ni_{60}Nb_{20}Zr_{20})_{30}$ powders was performed and the result is shown in Fig. 7. When annealing at 723 K, only a flat curve was observed, indicating the incubation time for crystallization at this temperature is larger than 30 min. Based on this result, the vacuum hot-pressing temperature was set at 723 K, which is ~10 K higher than the first $T_g$ of dual-amorphous-phased $(Ti_{50}Cu_{28}Ni_{15}Sn_7)_{70}(Ni_{60}Nb_{20}Zr_{20})_{30}$ powders. Figure 8 shows a typical BA/AC alloy disc prepared by vacuum hot pressing amorphous $Ti_{50}Cu_{28}Ni_{15}Sn_7$ powders with 30 vol% of amorphous $Ni_{60}Nb_{20}Zr_{20}$ addition. The cross-sectional view of the corresponding disc sample examined by SEM is also shown in Fig. 8. Two phases are observed in the SEM image. In addition, some residual porosity among the amorphous phases was also observed. The main reason for it is probably due to the low temperature or short time of hot-pressed process. Meanwhile, the cross-sectional views of the corresponding powders before and after consolidation into a disc were examined by SEM and the results are shown in Fig. 9. Figure 9a reveals that some amorphous powders were encapsulated by the other amorphous phases. Since the amorphous $Ti_{50}Cu_{28}Ni_{15}Sn_7$ phase exhibited a lower microhardness than that of $Ni_{60}Nb_{20}Zr_{20}$, the inner part would be hard particles of $Ni_{60}Nb_{20}Zr_{20}$ and this would be surrounded by $Ti_{50}Cu_{28}Ni_{15}Sn_7$ soft matrix (also host matrix). Similar behaviour has been reported on the preparation of $SiC_p$/Al metal matrix composite by high-energy ball-milling process [11]. The SEM image of the amorphous composite powders confirmed the DSC observation (Fig. 6) of dual-phase amorphous alloy powders. After consolidation into a disc, as shown in Fig. 9b, the $Ni_{60}Nb_{20}Zr_{20}$ particles are observed to have distributed uniformly within the $Ti_{50}Cu_{28}Ni_{15}Sn_7$ matrix. Energy-

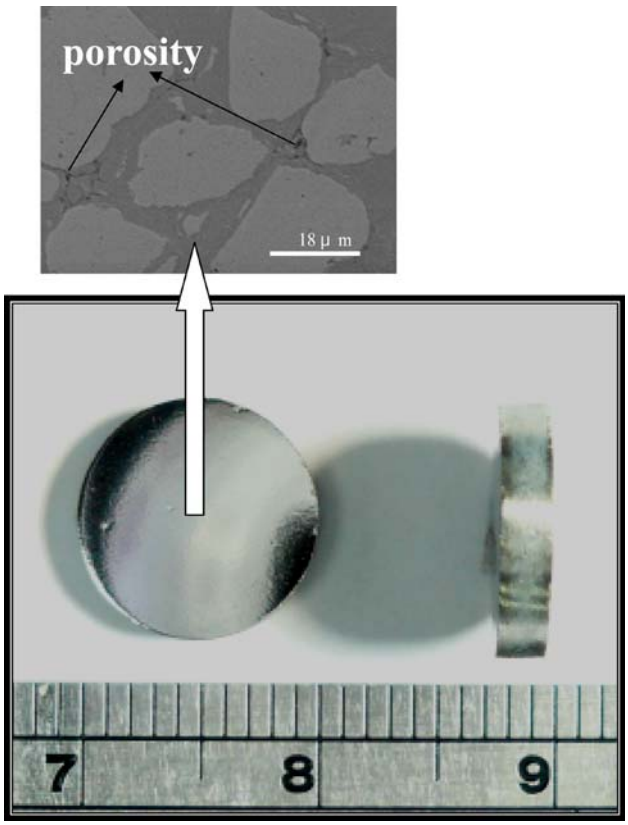


**Fig. 8** Optical micrograph and cross-sectional view of a $(Ti_{50}Cu_{28}Ni_{15}Sn_7)_{70}(Ni_{60}Nb_{20}Zr_{20})_{30}$ DAPBMG disc

dispersive spectroscopy was performed and it confirmed the above discussion; however, the results are not shown here.

The amorphization status of the BA/AC alloy discs, however, was re-examined by TEM, and the corresponding bright-field (BF) image and SAD pattern are shown in Fig. 10. The BF image of $(Ti_{50}Cu_{28}Ni_{15}Sn_7)_{70}(Ni_{60}Nb_{20}Zr_{20})_{30}$ disc sample as shown in Fig. 10a reveals a typical "salt-and-pepper" microstructure representing a homogeneous amorphous phase. The inset shown in Fig. 10b presents the SAD pattern taken from the matrix, which shows a typical amorphous pattern characterized by a diffuse halo ring. This implies that the BA/AC alloy was prepared successfully by hot pressing the corresponding composite powders at 723 K under a pressure of 1.2 GPa. The bulk density values of the $(Ti_{50}Cu_{28}Ni_{15}Sn_7)_{100-x}(Ni_{60}Nb_{20}Zr_{20})_x$ BA/AC disc as measured by the Archimedean method are in the range of 6.634–6.880 g/cm$^3$, while that for $Ti_{50}Cu_{28}Ni_{15}Sn_7$ and $Ni_{60}Nb_{20}Zr_{20}$ discs consolidated with the same manner are 6.461 and 7.751 g/cm$^3$. The linear increase of density values suggests that the overall bulk density of BA/AC alloys can be described by a rule of mixtures [12]. The mechanical property of BA/AC alloy samples was evaluated by the Vickers microhardness

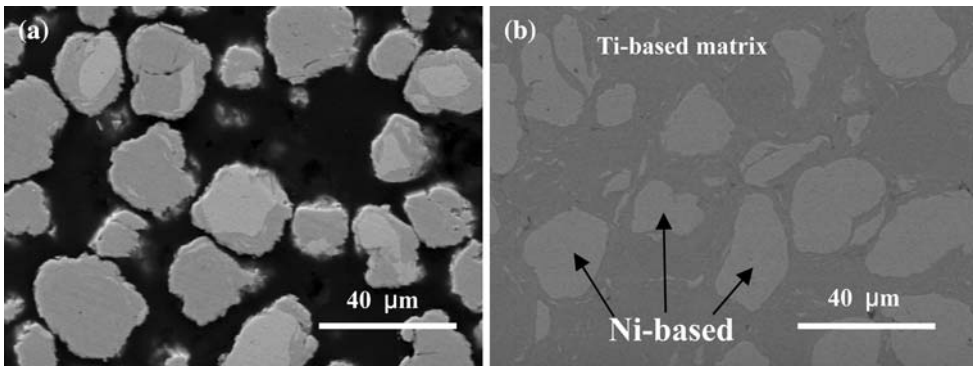


**Fig. 9** SEM cross-sectional views of amorphous composite $(Ti_{50}Cu_{28}Ni_{15}Sn_7)_{70}(Ni_{60}Nb_{20}Zr_{20})_{30}$ powders (**a**) before and (**b**) after vacuum hot pressing

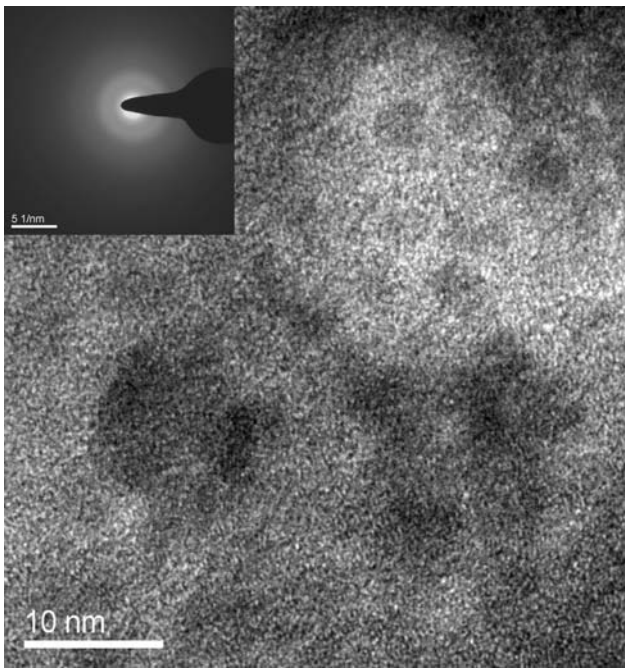


**Fig. 10** TEM (**a**) bright-field image and (**b**) selected area diffraction pattern of $(Ti_{50}Cu_{28}Ni_{15}Sn_7)_{70}(Ni_{60}Nb_{20}Zr_{20})_{30}$ BA/AC alloy disc

tests. Because a relatively high density had been achieved, the influence of porosity could be neglected for $Ti_{50}Cu_{28}Ni_{15}Sn_7$ BMG, and its BA/AC investigated in the present study. The Vickers microhardness increased from 669 Kg/mm$^2$ for $Ti_{50}Cu_{28}Ni_{15}Sn_7$ BMG to 686, 710, and 726 Kg/mm$^2$ for BA/AC alloys with 10, 20, and 30 vol% $Ni_{60}Nb_{20}Zr_{20}$ additions, respectively. Though the differences in bulk density may have affected the microhardness of the BA/AC alloy discs, the Vickers microhardness of the BA/AC alloy discs conformed to the general mixture rule [12].

## Conclusion

A $(Ti_{50}Cu_{28}Ni_{15}Sn_7)_{100-x}(Ni_{60}Nb_{20}Zr_{20})_x$ ($x = 0, 10, 20$, and 30 vol%) BA/AC alloy was prepared successfully through the vacuum hot pressing of their corresponding mechanically alloyed amorphous powders. Microstructural observation revealed that the amorphous $Ni_{60}Nb_{20}Zr_{20}$ phase is distributed uniformly within the amorphous $Ti_{50}Cu_{28}Ni_{15}Sn_7$ matrix. A single amorphous peak was observed for dual-amorphous-phased $(Ti_{50}Cu_{28}Ni_{15}Sn_7)_{100-x}(Ni_{60}Nb_{20}Zr_{20})_x$ powders, and its position increased with the $Ni_{60}Nb_{20}Zr_{20}$ concentration. The Vickers microhardness was 669 Kg/mm$^2$ for $Ti_{50}Cu_{28}Ni_{15}Sn_7$ BMG and increased to 686, 710, and 726 Kg/mm$^2$ for the BA/AC alloy containing 10, 20, and 30 vol% $Ni_{60}Nb_{20}Zr_{20}$, respectively. Though the differences in bulk density may have affected the microhardness of the BA/AC alloy discs, the Vickers microhardness of the BA/AC alloy discs conformed to the general mixture rule.

## References

1. Davidson DL (1991) Metall Trans A 22A:113
2. Choi-Yim H, Johnson WL (1997) Appl Phys Lett 71:3808
3. Kuhn U, Eckert J, Mattern N, Schultz L (2002) Appl Phys Lett 80:2478
4. Wilde G, Rosner H (2007) J Mater Sci 42:1772
5. Li F, Zhang T, Guan S, Shen N (2005) Mater Lett 59:1453
6. Mattern N, Kuhn U, Gebert A, Gemming T, Zinkevich M, Wendrock H, Schultz L (2005) Scripta Mater 53:271
7. Park ES, Jeong EY, Lee JK, Bae JC, Kwon AR, Gebert A, Schultz L, Chang HJ, Kim DH (2007) Scripta Mater 56:197
8. Lin HM, Lin CK, Jeng RR, Bor HY, Lee PY (2008) Metall Mater Trans A (in press)
9. Annual book of ASTM standards, ASTM C693-84 (1991) p 221
10. Lee PY, Yang JL, Lin HM (1998) J Mater Sci 33:235
11. El-Eskandarany MS (1998) J Alloys Comp 279:263
12. Doglione R, Spriano S, Battezzati L (1997) Nanostructured Mater 8:447